PROCEEDINGS, 41st Workshop on Geothermal Reservoir Engineering
Stanford University, Stanford, California, February 22-24, 2016
SGP-TR-209

Hydro-Mechanically Coupled Flow through Heterogeneous Fractures

D. Vogler, R. Settgast, C. Annavarapu, P. Bayer and F. Amann

ETH Zurich, Sonneggstr. 5, 8092 Zurich, Switzerland

daniel.vogler@erdw.ethz.ch

Keywords: heterogeneous fractures – fracture flow – fracture mechanics

ABSTRACT

Heterogeneous aperture distributions are an intrinsic characteristic of natural fractures. The presence of highly heterogeneous aperture distributions can lead to flow channeling, thus influencing the macroscopic behavior of the fluid flow. High-fidelity numerical simulation tools are needed for realistic simulation of fracture flow when such features are present. Here, focus is set on the role of mechanical fracture closure for fluid flow and appropriate simulation by a fully hydro-mechanically (HM) coupled numerical model. In a laboratory experiment, an artificial fracture in a granodiorite sample is created. During different sequential loading cycles, the development of fracture closure, contact area and contact stress are examined. Constant fluid flow rate injection into the center of the rough fracture is modelled to investigate the impact of fracture closure on the flow field and injection pressure. Results show that the numerical framework for heterogeneous fracture surfaces allows for reproducing experimental data of dry, mechanical tests at the laboratory scale, and it may offer advanced understanding and prediction of the behavior of reservoirs that are subject to high-pressure fluid injections.

1. INTRODUCTION

Geothermal reservoir productivity strongly depends on fracture network and single fracture permeability. Fracture aperture and therefore reservoir permeability are subject to changes in the lifetime of an enhanced geothermal system as a consequence of cold fluid injections in a hot reservoir (Min et al. 2004, McDermott et al. 2006, Koh et al. 2011, Fox et al. 2015). Associated effective normal stress changes, dilatant shearing and thermo-elastic effects affect both reservoir productivity and related seismic risk. For description of the governing processes, computationally demanding hydro-mechanically (HM) coupled models are frequently used (Baghbanan and Jing 2008, Nemoto et al. 2009, Rutqvist 2011). Alternatively, simplifications such as the assumption of planar fractures rather than heterogeneous fractures are suggested (Gangi 1978, Hayashi et al. 1999, Riahi and Damjanac 2013). However, such simplifications are not always representative of reservoir characteristics and it is desirable to explicitly model fracture heterogeneities.

The GEOS modeling framework enables to explicitly account for complex fracture surface geometries and its influence on coupled fracture flow. GEOS is a massively parallel simulation framework developed at Lawrence Livermore National Laboratory. It is a fully-coupled finite element/finite volume approach to model hydraulically driven fractures with arbitrary 3D geometries and facilitates a realistic representation of local heterogeneities, layering and natural fracture networks in a reservoir (Settgast et al. (2016)). Recently, for example Guo et al. (2016) utilized a thermo-hydro-mechanically (THM) coupled model developed in GEOS for inspecting the role of flow channeling in a large-scale heterogeneous fracture for the long-term energy production of a geothermal reservoir. In our study, a GEOS HM-coupled model is compared to small-scale experimental observations to investigate heterogeneous fracture mechanics. We scrutinize simulations of flow velocity field evolution during different normal loading scenarios on a fracture of a crystalline rock specimen. The model is tested for normal stresses up to 70 MPa, which results in fluid pressures above 10 MPa in individual cases. This enables detailed investigation of the normal stress-dependent flow channeling, the increase of contact area and contact stress with rising normal stresses, and fracture opening at high fluid pressures. In the following, first the experimental setup and results are presented. Then, we inspect fracture normal closure and associated aperture field evolution in a fully HM-coupled fracture simulation.

2. EXPERIMENTAL AND NUMERICAL INVESTIGATION OF FRACTURE PROCESSES

2.1 Experimental setup

A cylindrical granodiorite rock sample from the Grimsel Deep Underground Lab, Switzerland, with 200 mm height and 122 mm diameter was used for this study. Normal to the specimen, a fracture was induced by loading two saw-cut notches with a millimeter depth on opposite sides of the specimen with two prisms. The specimen was loaded to investigate fracture closure, stress distribution in the fracture and changes in aperture fields. First, the sample was equipped with a DD1 sensor at the fracture to measure fracture closure and deformation of the intact material in axial direction between the top and bottom of the sample. The axial load across the artificial fracture in the center of the specimen was increased from 0.14 to 10 MPa and subsequently decreased to 0.14 MPa using a 2000 kN servo-controlled Walter and Bai rock testing device.

Fracture and intact rock mass deformation measured during the experiment were separated by calculating the theoretical intact rock deformation with the Young's modulus measured for the core material. Pressure sensitive film from FUJI (FUJI pre-scale film) as used by Selvadurai and Glaser (2015) was then placed in the fracture, which was loaded to thirteen different stress states between maximum and minimum axial stress. Three different films with different pressure sensitivities between 0.5-2.5, 2.5-10 and 10-50 MPa were used to obtain a large range of contact stresses within the fracture. The lower stress range margin denotes stress levels that can be detected by the film while the higher stress range margin denotes the maximum stress state that can be differentiated from the stress range. All

values higher than this maximum range are assigned the maximum stress state. The stress states measured on the pressure-sensitive films were superposed to obtain a stress map in the fracture between 0.5 to 50 MPa.

Figure 1: Specimen during testing with pressure sensitive foil

2.2 Experimental results

2.2.1 Fracture normal closure

Fracture closure is measured with a sensor that is positioned 2.5 cm above and below the fracture, at opposite sides of the specimen. The sensor gives relative displacement between the upper and lower sensor part. This displacement is depicted in the green curve in Figure 2. Displacement is larger for lower stresses and starts to converge for higher stress levels. For the maximum axial confining stress of 10 MPa, a displacement of 0.16 mm is reached. After reaching the maximum axial confining stress of 10 MPa, the sample is unloaded, during which irreversible displacement becomes apparent. After fully unloading the sample, an irreversible displacement of 0.55 mm remains, which can largely be attributed to irreversible fracture closure, since the intact rock mass is expected to behave elastically in this stress regime.

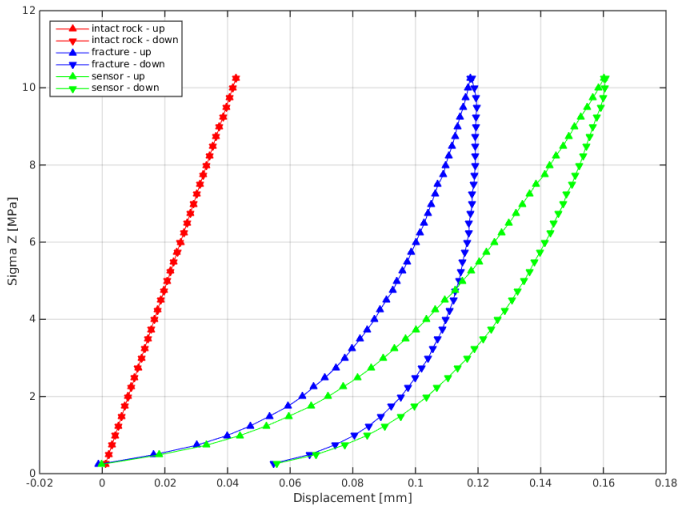

Figure 2: Measurements of displacement (deformation) of sensor 2.5 cm above and below fracture (green), and derived compression of intact rock (red) and fracture (blue).

Measurements of static e-Modulus on intact rock samples of the same core meter enable calculation of the theoretical elastic deformation and show the completely elastic deformation of the sample during loading and unloading. Thus, obtained elastic displacement expected between the upper and lower sensor parts is shown in red in Figure 2. The irreversible fracture deformation can be calculated from the sensor measurements and the intact rock mass deformation and is shown in blue in Figure 2. With increasing axial confining stress, the displacement changes (i.e. fracture closure) become smaller while the elastic intact rock mass deformation increases linearly. The convergent behavior of fracture closure is also documented in the literature, e.g., Barton et al. (1985). This phenomena can be explained with increasing contact area in the fracture as load increases until the fracture aperture reaches a residual value and further increase in stress is taken up by the surrounding rock mass. During unloading, the fracture does not open to the original position. While the fracture reopens elastic asperity deformation, increased mating, shear displacement and small plastic or brittle deformations of asperities can lead to irreversible fracture opening during unloading.

2.2.2 Aperture field

Fracture surfaces were scanned with the high-resolution photogrammetry scanner ATOS Core 3D by GOM. The ATOS core sensor projects fringe patterns onto the fracture surface, which are detected by two cameras. The phase shift patterns based on sinusoidal intensity distribution enable a derivation of a three-dimensional surface. The aperture field derived from matching both surface scans of the fractures is shown in Figure 3a. The field shows three (reddish) regions with small aperture values that are anticipated to provide most contact. Multiple patches in the fracture have an aperture larger than 1 mm, which is chosen as the largest value to depict in the color bar since areas with a larger aperture are not expected to close during loading. The histogram of the aperture distribution in Figure 3b follows approximately a log-normal distribution with most aperture values below 0.5 mm.

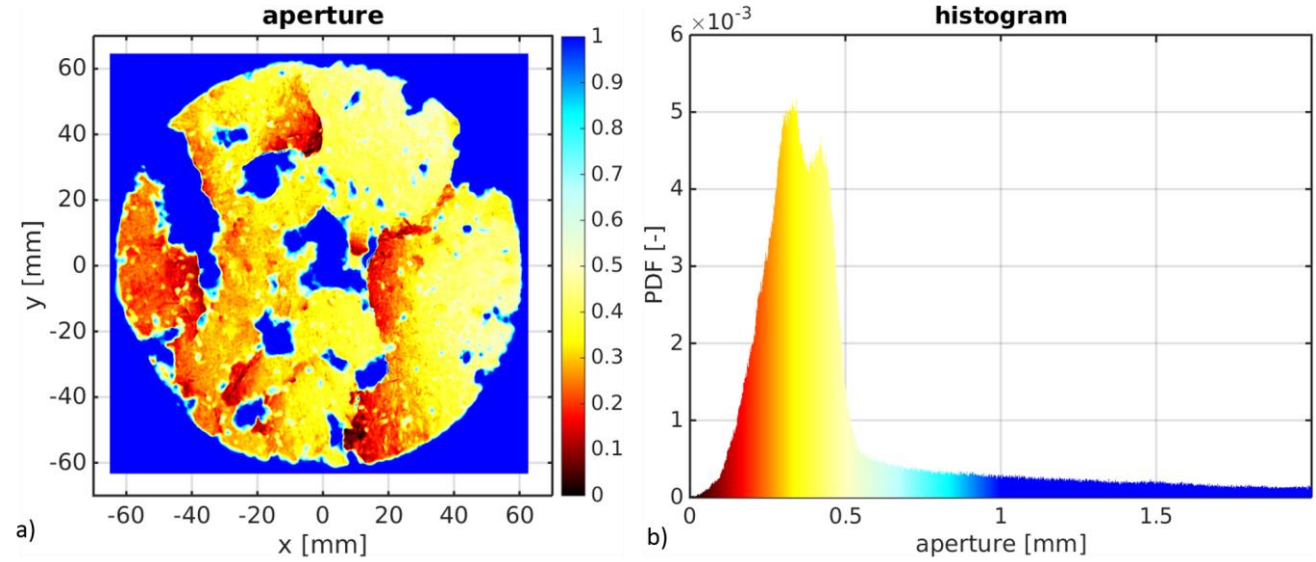

Figure 3: Fracture aperture field as seen from above (left) and histogram of aperture distribution (right).

2.2.3 Contact stresses

The contact stress evolution in the fracture as measured with the pressure sensitive film is depicted in Figure 4. Contact stress evolution is shown for 0.25, 5 and 10 MPa (Figure 4a, b and c, respectively). Normal stresses for 0.25 MPa show a homogeneous distribution across the fracture, with maximum stresses below 3 MPa. Due to the thickness of 200 µm of the pressure sensitive film, normal stress is not expected to be solely concentrated in a few contact points, but more evenly across the fracture. Regions with very low apertures (Figure 3a – black and dark red colored area) are visible as areas with stress concentrations for 0.25 MPa axial stress. With 5 MPa normal stress on the specimen in axial direction, normal stresses in the fracture show that the fracture is largely closed in most areas except high aperture areas also visible in Figure 3. This becomes apparent in the drastic increase of contact area with low stresses (light blue color in Figure 4a). From 5 to 10 MPa, scan results show a small increase in low-stress contact areas, with the majority of changes occurring in high-stress regions (Figure 4c) that align with low aperture regions in Figure 3a. High aperture regions visible in blue in Figure 3a now emerge as the remaining areas with no contact stresses above 0.5 MPa and are clearly visible in Figure 4c.

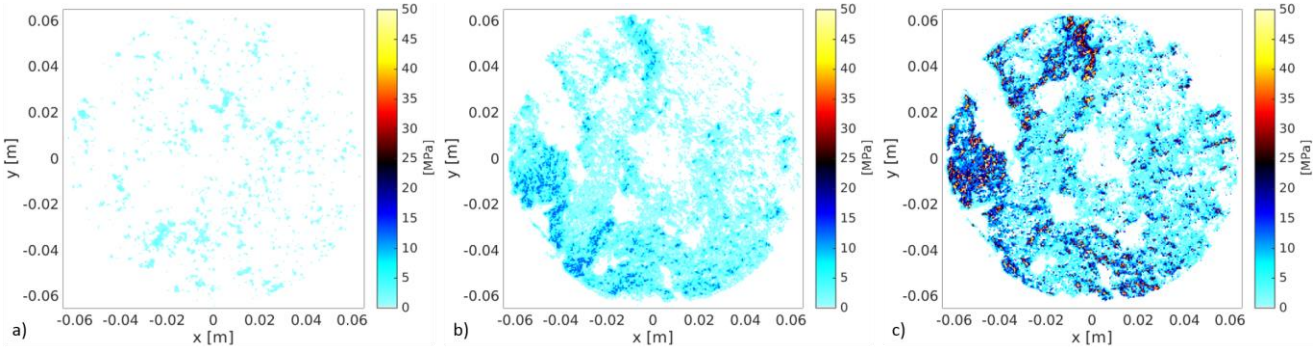

Figure 4: Measured normal stress in fracture for normal stresses of a) 0.5, b) 5.0 and c) 10 MPa.

2.3 Methodology of numerical simulations

The GEOS framework developed at LLNL was used to simulate HM-coupled processes in heterogeneous fractures. First, fracture mechanics were simulated dry, without fluid flow, to compare simulation results to experimental results of sample deformation from which intact rock deformation and fracture closure can be separated. The geometry of the cylinder was simulated with increasing

confining stress in axial direction. The aperture field used for mechanics and fluid flow in the fracture was obtained from matched surface scans of the fracture (Figure 3a). Additionally, mechanics and fluid flow for a constant injection rate into the fracture center with constant atmospheric pressure at the fracture boundaries was simulated, resulting in radial flow from the fracture center outwards.

2.4 Numerical results

2.4.1 Fracture normal closure

Displacement in the numerical model was read out for the respective sensor locations on the specimen in the experiment. The displacement obtained from simulations was compared to the experimental results and is shown in Figure 5a. Fracture closure is based on the aperture field as derived from the photogrammetry scans and the rock properties measured in the experiment. A fracture normal stiffness K_N can be obtained from the experimental data by relating fracture closure u_N to normal stress increase σ_N with a linear relation ($K_N = d\sigma_N/du_N$). This normal stiffness represents an averaged property across the whole fracture, which changed by an order of magnitude during the experiment when relating displacement changes for low vs. high stresses. The value obtained from experimental data was used as a starting point to arrive at a normal stiffness that represents fracture contact behavior. Modelling fracture closure with a homogeneous aperture distribution and a constant normal stiffness leads to the expected linear relation between fracture closure and confining stress (not shown here). However, when using the heterogeneous aperture field within the fracture (Figure 3a), the contact area in the model increases with confining stress, which leads to the non-linear behavior observed in Figure 5a.

2.4.2 Aperture field evolution

Aperture probability distributions in the fracture from the numerical model without fluid flow were recorded for individual load stages (Figure 5b). Results show a shift of the aperture field to lower values from 0.25 MPa to 10 MPa confining stress. Additionally, the high probability region that can be seen in Figure 5b between apertures of 0.15 and 0.35 mm is compacted with rising stress as the amount of contact area in the fracture increases.

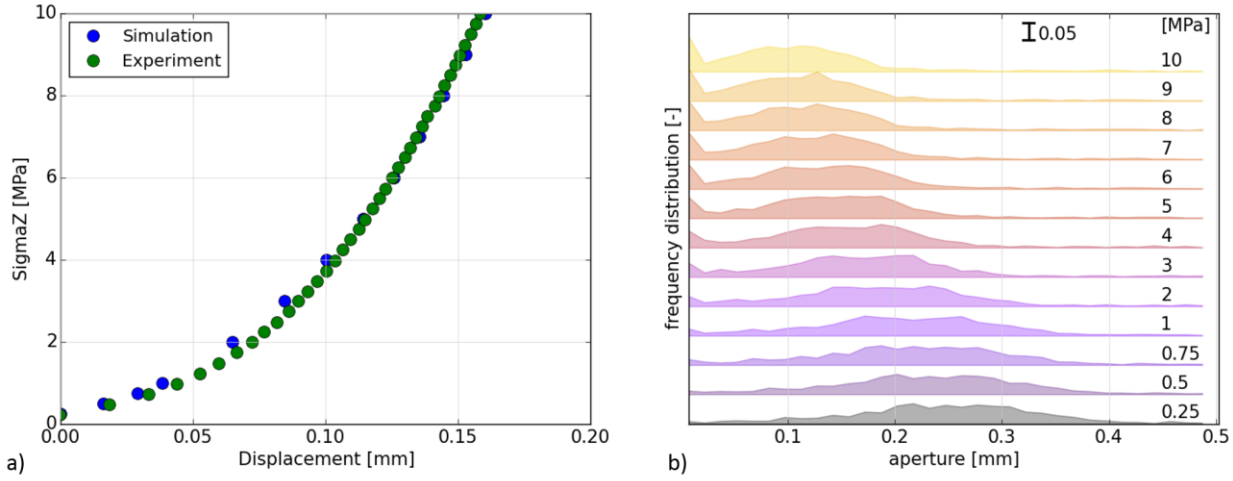

Figure 5: a) Results for displacement between top and bottom part of sensor (consisting of compression of intact rock and fracture in both experiment and simulation) and b) aperture field in fracture for confining stress between 0.25 and 10 MPa.

2.4.3 Fully HM-coupled fracture flow simulation

Figure 6 shows the evolution of aperture (Figure 6, left column), velocity field (Figure 6, middle column) and pressure (Figure 6, right column) for 0.25, 5 and 10 MPa (Figure 6a, b and c respectively) axial confining stress. The color bar shown in Figure 6d is used for all three stress levels and kept constant. The aperture field shows scattered regions of high aperture across the fracture plane. High aperture regions (above 1 mm) found across the fracture serve as connecting fluid channels (Figure 6, middle column). Medium aperture regions (between 0.1 and 0.6 mm) close with increasing confining stress and for high stresses, only large aperture regions above 0.6 mm remain open with medium aperture areas closing to aperture values below 0.15 mm. Regions with high aperture values (above 1 mm) that remain open for large stresses are also apparent as no-contact regions on the measurements made on pressure sensitive film (Figure 4b-c). For low stress (0.25 MPa - Figure 6a) fluid flow occurs along four wide channels, which become narrower when the fracture closes. One major flow channel, which is not fully developed for low stresses, forms at the bottom end of the fracture for high stresses. Due to the constant flow rate, the velocity field does not change completely, while the injection pressure required to sustain constant flow rates across axial stresses changes drastically. The contact area (i.e. low aperture area) to the right of the fracture center is clearly visible as a no-flow region (Figure 6, center) and a region with strong pressure gradients (Figure 6, right column). Areas of large aperture (Figure 3a

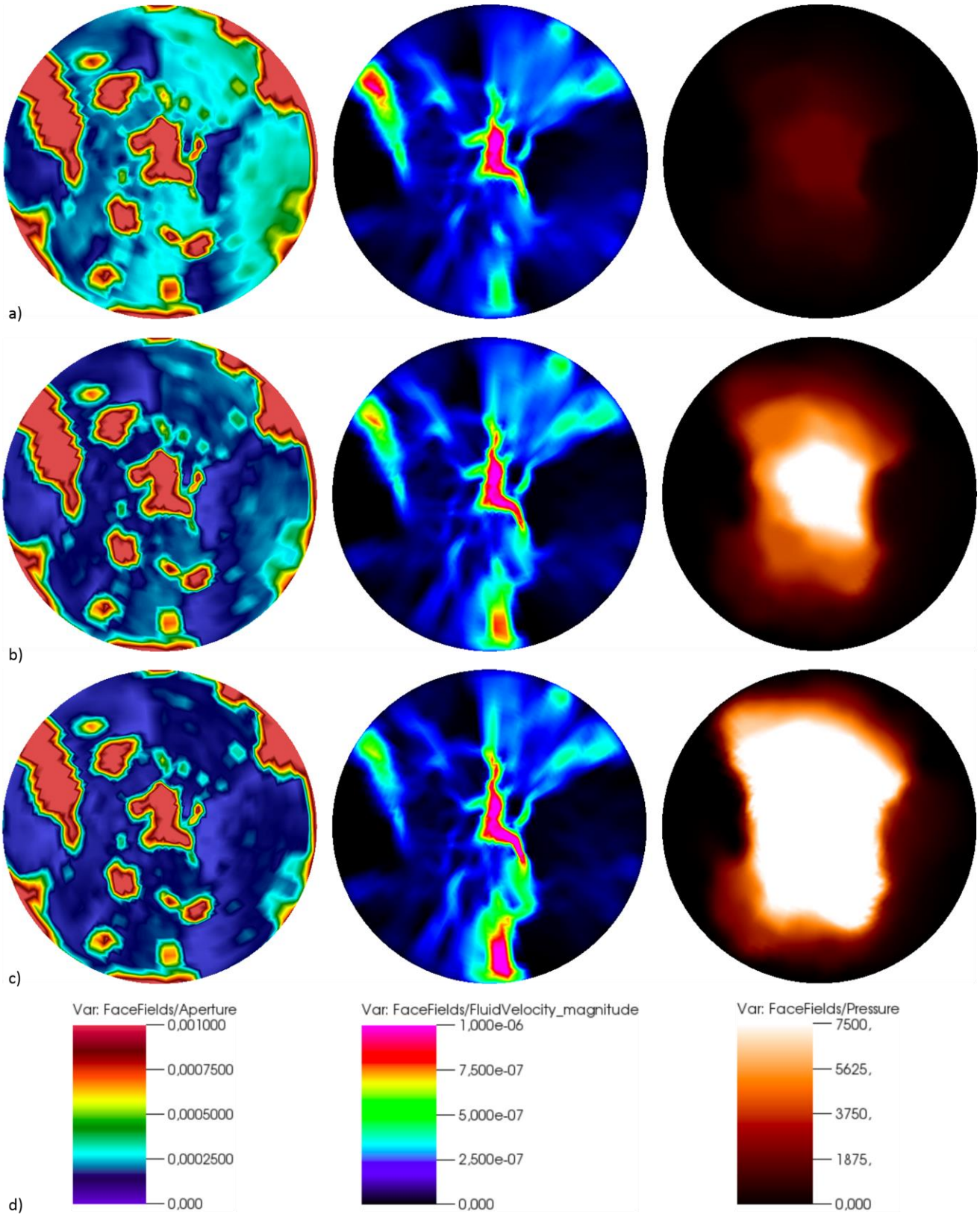

Figure 6: Aperture field (left column, in m), velocity field (middle, in m^3/s) and pressure distribution (right, in Pa) within a heterogeneous fracture. Changes in pressure for a) 0.25 MPa, b) 5 MPa, and c) 10 MPa are shown. The legend is shown in d).

and 6) emerge as regions with large fluid velocity and most fluid channels are formed by connecting areas with large apertures. The predominant flow channels under high axial load emerge above and below the fluid injection in the middle of the fracture. These regions of high aperture can be seen in the aperture field derived from surface scans in figure 3a.

CONCLUSIONS

Experiments on hydro-mechanical processes in artificially induced tensile fractures were performed. Results show convergent behavior for fracture closure, with rapid fracture closure during increasing axial stresses up to 5 MPa. Towards the maximum axial stress of 10 MPa, fracture closure converges to 0.16 mm at 10 MPa axial stress. During unloading, fracture closure is shown to be irreversible with an irreversible closure of about 0.05 mm. Results of pressure sensitive film loaded within the fracture achieved a good representation of high-stress and no-stress regions that closely correlate with low-aperture and high-aperture regions of the aperture fields. A hydro-mechanical module in the GEOS framework was used to model fracture closure and fluid pressure response during compression. Fracture heterogeneities were successfully included in the model by using an aperture field derived from photogrammetric scans of the fracture surfaces. Modeling dry fracture closure yields good agreements with experimental measurements, replicates the convergent behavior observed during fracture closure in experiments and allows quantitative analysis of the aperture field distribution. Simulations of changes in fluid flow field and injection pressure under loading of the heterogeneous fracture show the evolution of flow channels and give insight into injection pressure response to changes in effective confining stresses on a fracture.

ACKNOWLEDGEMENTS

The authors would like to thank the Chair of Geosensors and Geodesy at ETHZ and especially Robert Presl for their help with the photogrammetry scanner. This work was partially be supported by the GEOTHERM II project in the ETH domain.

REFERENCES

Barton, N., and Bandis, S. and Bakhtar, K.: Strength, Deformation and Conductivity Coupling of Rock Joints, *Int. J. Rock. Mech. Min. Sci. and Geomech. Abstr.* , **22**, (1985), 121-140.

Selvadurai, P. A., and Glaser, S. D.: Laboratory-developed contact models controlling instability on frictional faults, *J. Geophys. Res. Solid Earth*, **120**, (2015), 4208-4236.

McDermott, C. I., Randriamanjatosoa, A. R., Tenzer, H., & Kolditz, O. (2006). Simulation of heat extraction from crystalline rocks: The influence of coupled processes on differential reservoir cooling. Geothermics, 35(3), 321-344.

Fox, D. B., Koch, D. L., & Tester, J. W. (2015). The effect of spatial aperture variations on the thermal performance of discretely fractured geothermal reservoirs. Geothermal Energy, 3(1), 1-29.

Min, K. B., Rutqvist, J., Tsang, C. F., & Jing, L. (2004). Stress-dependent permeability of fractured rock masses: a numerical study. International Journal of Rock Mechanics and Mining Sciences, 41(7), 1191-1210.

Baghbanan, A., & Jing, L. (2008). Stress effects on permeability in a fractured rock mass with correlated fracture length and aperture. International Journal of Rock Mechanics and Mining Sciences, 45(8), 1320-1334.

Nemoto, K., Watanabe, N., Hirano, N., & Tsuchiya, N. (2009). Direct measurement of contact area and stress dependence of anisotropic flow through rock fracture with heterogeneous aperture distribution. Earth and Planetary Science Letters, 281(1), 81-87.

Koh, J., Roshan, H., & Rahman, S. S. (2011). A numerical study on the long term thermo-poroelastic effects of cold water injection into naturally fractured geothermal reservoirs. Computers and Geotechnics, 38(5), 669-682.

Hayashi, K., Willis-Richards, J., Hopkirk, R. J., & Niibori, Y. (1999). Numerical models of HDR geothermal reservoirs—a review of current thinking and progress. Geothermics, 28(4), 507-518.

Riahi, A., & Damjanac, B. (2013). Numerical study of hydro-shearing in geothermal reservoirs with a pre-existing discrete fracture network. In Proceedings of the 38th Workshop on Geothermal Reservoir Engineering, Stanford, CA (pp. 11-13).

Guo, B., Fu, P., Hao, Y., Peters, C. A., & Carrigan, C. R. (2016). Thermal drawdown-induced flow channeling in a single fracture in EGS. Geothermics, 61, 46-62.

Rutqvist, J. (2011). Status of the TOUGH-FLAC simulator and recent applications related to coupled fluid flow and crustal deformations. Computers & Geosciences, 37(6), 739-750.

Gangi, A. F. (1978). Variation of whole and fractured porous rock permeability with confining pressure. In International Journal of Rock Mechanics and Mining Sciences & Geomechanics , 15, 5, 249-257.

Settgast, R. R., Fu, P., Walsh, S., D., C., White, J., A., Annavarapu, C., Ryerson, F., J. (2016). A Fully Coupled Finite Element/Finite Volume Method for the Massively Parallel Simulation of Hydraulically Driven Fractures in 3-Dimensions. In International Journal for Numerical and Analytical Methods in Geomechanics, under review.